The ^{12}C+^{24}Mg elastic scattering:
An example of anomalous transparency
at Coulomb barrier energies [*]

W. Sciani [a,*], A. Lépine-Szily [a], R. Lichtenthäler F. [a], P. Fachini [a,*],
L.C. Gomes [a], G.F. Lima [a,*], M.M. Obuti [b,*], J.M. Oliveira Jr. [c,*],
A.C.C. Villari [d]

[a] *IFUSP-Universidade de São Paulo, C.P.66318, CEP 05315-970, São Paulo, Brazil*
[b] *SPring-8, Synchrotron Radiation Research Institute, Kamigori cho, Ako gun, Hyogo 678-12, Japan*
[c] *Departamento de Ciencias Exatas e Naturais da Universidade de Sorocaba, C.P. 578, 18060-000,
Sorocaba, Brazil*
[d] *GANIL, B.P. 5027, 14021 Caen Cedex, France*

Abstract

Fifteen complete angular distributions of the elastic scattering of ^{12}C+^{24}Mg were measured at energies around the Coulomb barrier (E_{cm} = 10.67–16 MeV). The angular distributions are strongly oscillating and could be well described by an optical potential family, whose real part was determined without continuous ambiguity. The imaginary part of this optical potential is very shallow. At four energies the inelastic scattering angular distributions leading to the 2^+ state of the ^{24}Mg were also measured and analysed with coupled-channels calculations. The volume integrals of the optical potentials used in the coupled-channels calculations present the threshold anomaly in their energy dependence, with a clear Q-value dependence. © 1997 Elsevier Science B.V.

PACS: 25.70.Lm; 24.10.Eq; 25.70.Hi; 25.70.Jj
Keywords: Elastic scattering; Inelastic scattering; Optical model analysis; Threshold anomaly; Coupled channels calculations; Optical potential; Potential ambiguity.

1. Introduction

In a recent letter [1], we reported the measurements and optical model analysis of the complete angular distributions of the elastic scattering of ^{12}C+^{24}Mg at three

---

energies near the Coulomb barrier, namely at E_{cm} = 12.67, 14.00, and 15.33 MeV. These angular distributions presented "anomalous" features, namely strong oscillations even at the lowest energy (which is at the Coulomb barrier), which could not be reproduced by optical potentials previously used for other light systems [2–8], but only by "anomalously" transparent optical potentials [1].

Why do we call our date anomalous, if oscillating elastic angular distributions are a common feature and well known for a long time? The reason is, that the presence of strong oscillations in asymmetric systems ($A_2 - A_1 = 12$) at such low energies ($E_{cm} < V_{CB}$) is not a common feature and can not be explained by trivial processes, such as the Mott scattering of identical nuclei (e.g. $^{12}C+^{12}C$, $^{14}N+^{14}N$, $^{16}O+^{16}O$) [6–8], or the elastic transfer of nearly symmetric systems (e.g. $^{12}C+^{13}C$, $^{16}O+^{18}O$ and $^{12}C+^{16}C$). The elastic scattering of identical nuclei (e.g. $^{12}C+^{12}C$, $^{14}N+^{14}N$, $^{16}O+^{16}O$) [6–8] shows oscillations in the angular distributions at energies near to the Coulomb barrier, due to the quantum interference between scattering amplitudes $f(\theta)$ and $f(\pi - \theta)$ (Mott scattering). These oscillations are reproduced by e.g. the Maher potential (V_0 = 17 MeV and W_0 = $(0.1 + 0.4E_{cm})$ MeV, W_0/V_0 = 0.1 for E_{cm} = 12.5 MeV), which is ten times more absorptive than our optical potential II. If the colliding system is nearly symmetric, differing by some nucleons ($^{12}C+^{13}C$, $^{16}O+^{18}O$) or by an α-particle ($^{12}C+^{16}C$), oscillations appear due to the quantum interference between the direct elastic amplitude and the elastic transfer amplitude [9]. Since the elastic transfer amplitude is proportional to the transfer spectroscopic factor, this process is important for nearly symmetric systems and negligible for highly asymmetric systems, as $^{12}C+^{24}Mg$.

Back-angle oscillations (ALAS) [10] in asymmetric n–α systems are well known phenomena at higher energies (E_{cm} = 1.5 − 2V_{CB}). They can be reproduced by surface transparent optical potentials (STP) [4], which do not reproduce our oscillations observed at the Coulomb barrier [1].

Some twenty years ago Carter et al. [11,12] have observed a very unusual feature in the inelastic scattering of $^{12}C+^{24}Mg$ and $^{16}O+^{24}Mg$ systems at energies near to the Coulomb barrier (E_{cm} = 14.00 and 16.00 MeV): a second minimum was seen at angles larger than the usual Coulomb nuclear interference minimum. Extensive DWBA and coupled-channels calculations could not reproduce this second minimum. These features have attracted interest at the time: Landowne and Wolter [13] have performed coupled-channels calculations for the $^{16}O+^{24}Mg$ system, also including the α-transfer channel $^{24}Mg(^{16}O,^{20}Ne)^{20}Ne$. The effect of the two-step elastic transfer, taken into account in their calculation, was too small, and could not explain the observed anomaly, even when amplified.

Mermaz et al. [14] have measured complete elastic scattering angular distributions of the $^{16}O+^{28}Si$ system, at energies at to the Coulomb barrier (E_{cm} = 18.67, 19.03, 19.5, and 20.12 MeV), and their low energy data also presented slight oscillations, which were not well reproduced by their optical model analysis. The data of Mermaz have been analysed by Kobos and Satchler [15], adding some ad hoc corrections to the folding potential. The data at higher energy ($E_{cm} \geqslant$ 20.83 MeV) were well fitted, but at low energy ($E_{cm} \leqslant$ 20.12 MeV) the calculations did not produce the observed

oscillations.

Energy and parity dependent optical potentials [16] were successful to explain the back angle oscillations at higher energies (twice the Coulomb barrier) in the $^{16}O+^{28}Si$ system, but could not reproduce the observed oscillations at energies near to the Coulomb barrier [1].

In order to deepen the understanding of the anomalous elastic and inelastic scattering of the $^{12}C+^{24}Mg$ system at energies at the Coulomb barrier, we have measured complete elastic angular distributions for the $^{12}C+^{24}Mg$ system at fifteen energies around the Coulomb barrier, namely at E_{cm} = 10.67, 11.33, 12.00, 12.33, 12.67, 13.00, 13.33, 13.67, 14.00, 14.33, 14.67, 15.00, 15.33, 15.67, and 16.00 MeV and four inelastic angular distributions at E_{cm} = 12.67, 13.67, 14.00, and 15.33 MeV. The results of these measurements together with optical model and coupled-channels calculations will be presented in this article.

2. Experimental method and results

The measurements were performed at the Pelletron Laboratory of the University of São Paulo, using a ^{12}C beam bombarding an isotopically enriched thin ^{24}Mg target (20 $\mu g/cm^2$), evaporated on thin carbon backing. The laboratory energies used in this experiment were varied between 16.0 and 24.0 MeV, with steps of 0.5 MeV. Three telescopes, consisting of proportional gas counters followed by Si surface barrier detectors, allowed the identification of the detected particles. The simultaneous measurement of the ^{12}C and the recoiling ^{24}Mg in the forward hemisphere, permitted us to cover the angular range from Θ_{cm} = 20° to 164°.

The fifteen elastic angular distributions are shown in Figs. 1–3, and they exhibit strong oscillations at almost all energies, with the exception of the lowest energy. The inelastic scattering data, where the ^{24}Mg nucleus is excited to its first 2^+ state, was measured at E_{lab} = 19.0, 20.5, 21.0, and 23.0 MeV, and the data of Carter et al. [11], measured at E_{lab} = 24.0 MeV, was also included in the analysis. The inelastic differential cross-sections were not measured at very forward angles, due to the difficulty in separating the inelastic peak from the elastic at very low energies and forward angles. For this reason the Coulomb nuclear interference minimum is hardly seen, but at larger angles several oscillations are present, similar to the results of Carter et al. [11,12].

3. Optical model analysis

The fifteen elastic angular distributions are shown in Figs. 1–3. The value of the Coulomb barrier is V_{CB} = 12.56 MeV if the Christensen–Winther Coulomb radius R_{CB} = $1.07(A_P^{1/3} + A_T^{1/3})$ + 2.72 fm [17] is used for estimation. The data present strong oscillations at this and even at lower energies, indicating that the Coulomb barrier is probably lower.
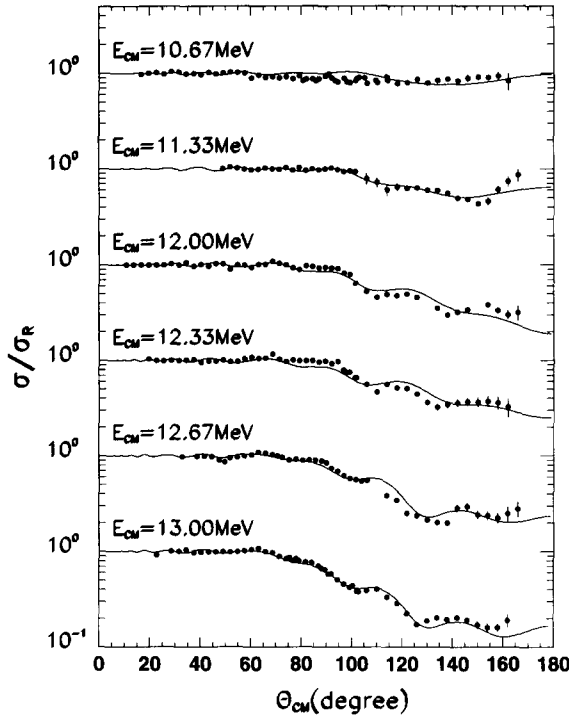
Fig. 1. The ^{12}C+^{24}Mg elastic scattering angular distributions, measured at the indicated energies, are represented by the dots. The solid lines are optical model calculations with our best fit optical potentials (Pot. II) of Table 1.

In our previous paper [1], we have discussed that when the shallow, energy-dependent, optical potential, which Siemssen et al. [2,3] used to fit light heavy ion elastic scattering at higher energy, ($V_0 = (7.5 + 0.5E_{cm})$ MeV, $W_0 = (0.4 + 0.15E_{cm})$ MeV, $r_0 = 1.35$ fm, and $a = 0.49$ fm) was extrapolated to our low energies ($E_{cm} = 10.67$–16.00 MeV), no oscillations were obtained at any of the measured energies. If the surface transparent (STP), energy-dependent optical potential of the Minnesota group [4], which gives a remarkable fit of the ^{16}O+^{28}Si elastic scattering angular distributions around $E_{cm} = 38$ MeV was extrapolated to our low energies, again we could not get any oscillations at any of the measured energies. The same holds for the energy-dependent potentials of Cheng [5] and Maher [6–8].

All of the optical potentials employed to fit these data, even very deep real potentials with a Woods–Saxon radial form-factor, failed to reproduce the oscillating angular distributions, unless the imaginary depth was reduced, not only on the surface but also in the nuclear interior to 1–2% of the real depth. However, if the depth of the imaginary part of any of the above cited optical potentials were just reduced, oscillations with the wrong period and phase would appear. The difficulty is to fit the oscillations at all energies with the correct phase and period. As a case of special difficulty, the angular distribution at $E_{cm} = 14.00$ MeV could not be fitted with any real potential depths
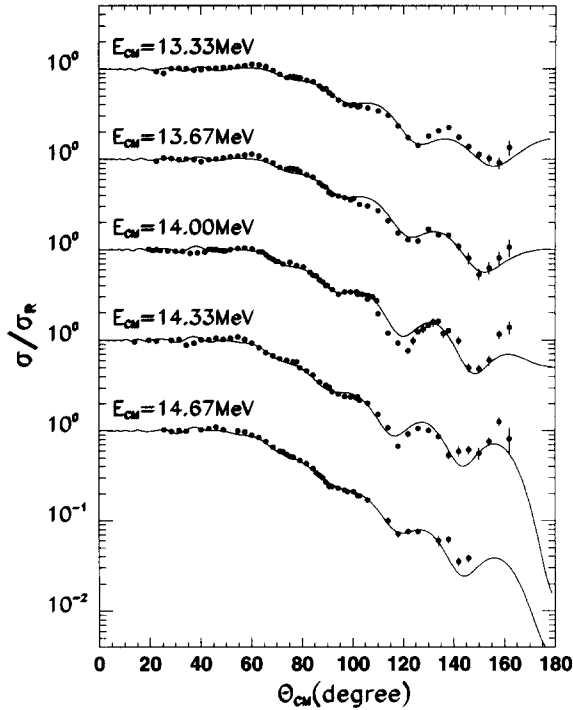
Fig. 2. The ^{12}C+^{24}Mg elastic scattering angular distributions, measured at the indicated energies, are represented by the dots. The solid lines are optical model calculations with our best fit optical potentials (Pot. II) of Table 1.

shallower than $V_0 \leqslant 30$ MeV.

It is also well known that at the Coulomb barrier the energy dependence of the potential depth is not a simple one, it is also called the threshold anomaly, and the real part can present a bell-shaped energy dependence (see Section 4). We were not concerned about finding a standard optical potential with a simple energy dependence, which would not fit well all the details of these data. For this reason and due to the great difficulty encountered in fitting the whole amount of data simultaneously with energy-dependent optical potentials, we performed a systematic parameter search independently, for three representative energies ($E_{cm} = 12.67$, 14.00 and 15.33 MeV) using the PTOLEMY [18] code with the following strategy [1]:

The V_0 and r_0 values were varied on a grid, respectively from 10 to 44 MeV, with steps of 1 MeV, and from 1.0 to 1.6 fm with steps of 0.02 fm, allowing a free variation of the real diffuseness parameter a and of the imaginary parameters W_0, r_{i0}, a_i by fitting the data. The results of this systematic search are shown in Fig. 4, which is a three-dimensional plot, where V_0, r_0 and $1/\chi^2$ are the axes, where χ^2 has the usual definition and measures the quality of the fit. The best fit parameters, producing oscillating cross-sections with good phase and period, correspond to low χ^2 values and peaks in the $1/\chi^2$ surface. The three surfaces, corresponding to the three incident energies, present discrete
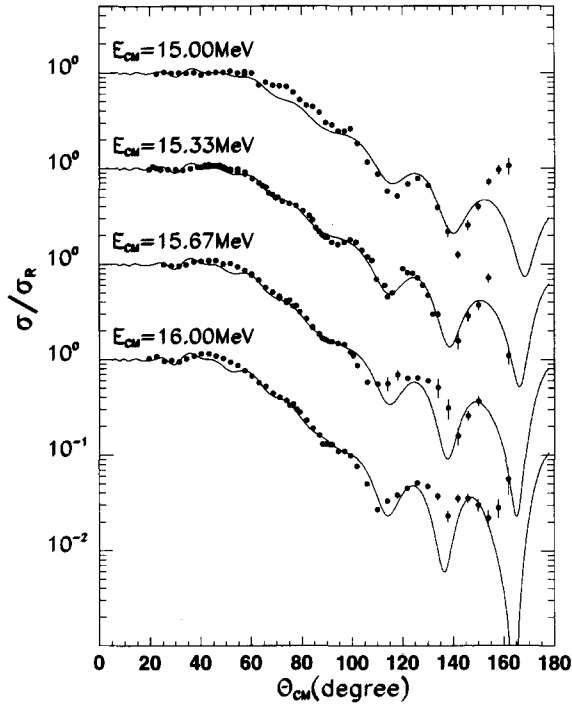
Fig. 3. The ^{12}C+^{24}Mg elastic scattering angular distributions, measured at the indicated energies, are represented by the dots. The solid lines are optical model calculations with our best fit optical potentials (Pot. II) of Table 1.
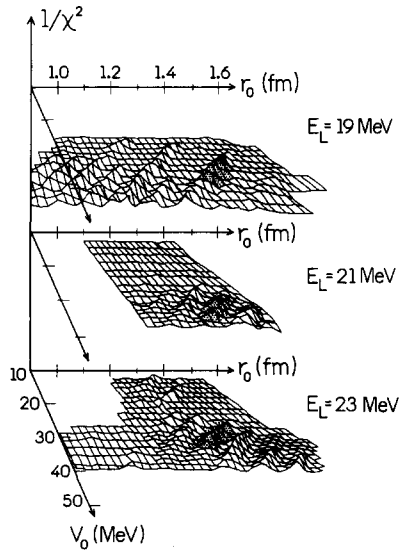

Fig. 4. Three-dimensional plots of the optical model parameters V_0, r_0 versus $1/\chi^2$, where χ^2 measures the quality of the fit.

"peaks", "mountains" for correlated (V_0, r_0) values, which are best fit real potential families and indicate that the V_0 (or r_0) parameters cannot be varied continuously and still find equally satisfying fits. In other words, there is no continuous ambiguity in the depth or the radius parameter of the real potential. The "peaks" are superimposed on plane regions, which correspond to completely smooth angular distributions, without oscillations, with nearly constant χ^2 values. For the parameter values of the plane regions the search procedure increased the W_0 imaginary depth, since otherwise there would be out-of-phase oscillations, with much worse χ^2 values.

The existence of only one "peak" in the $1/\chi^2$ plane at the same $r_0 = 1.29$ fm and approximately the same V_0 (difference less then 1 MeV, 3%) for the three energies (dotted peaks in Fig. 4) allows us to determine a unique potential in the studied parameter range, and within the reported constraints (r_0 independent of energy, conventional Woods–Saxon shape). It is interesting to note that the absence of "mountains" below $V_0 = 30$ MeV in the $1/\chi^2$ surface at $E_{\text{lab}} = 21.00$ MeV allowed us to conclude that at this energy the data cannot be reproduced by potentials with $V_0 \leqslant 30$ MeV. Among the Woods–Saxon shaped optical potentials, with energy independent radius, this is the first and shallowest real potential family, unique for $V_0 \leqslant 45$ MeV.

The best fit real potential parameters on the same "mountain" cross at well defined radial points (different potentials have the same depth, see Fig. 5), however not at the surface region, but at more internal points around 5.5 to 6.2 fm. The quantity which is maintained constant on the "mountain" is the volume integral of the potential and in Fig. 5 we present the potential families corresponding to different "mountains" with the values of their volume integrals:

$$J_V(E) = \left[\frac{4\pi}{A_{\text{T}} A_{\text{P}}} \int_0^R V(r, E) r^2 \, dr \right] . \tag{1}$$

For all three energies the best fit imaginary radius was $r_{i0} = 1.77$ fm, and the imaginary depth was very small ($W_0 < 1$ MeV) and energy dependent.

A search procedure executed blindly over all or part of the angular distributions, imposing a simple (linear or quadratic) energy dependence to the potential depths, without knowledge of the existence of these "peaks", could have connected by some spurious energy dependence "peaks" that do not belong to the same volume integral and the same potential family. The energy dependence near the Coulomb barrier should obey the threshold anomaly (see Section 4) and not simple linear or quadratic relations.

This same potential family was used as a starting point to reproduce the other twelve angular distributions. With the real geometry and the imaginary radius fixed, most angular distributions could be fitted just allowing a variation of the real and imaginary depths and the imaginary diffuseness in the search. Only for the three lowest energies we had to allow a variation of the real diffuseness in order to better the quality of the fits. The best fit optical model parameters (Pot. II) are presented on Table 1.

The variations in the real depth V_0 as a function of incident energy are rather small, between 0.3 and 2.5 MeV at maximum. Since the distance between discrete "mountains"
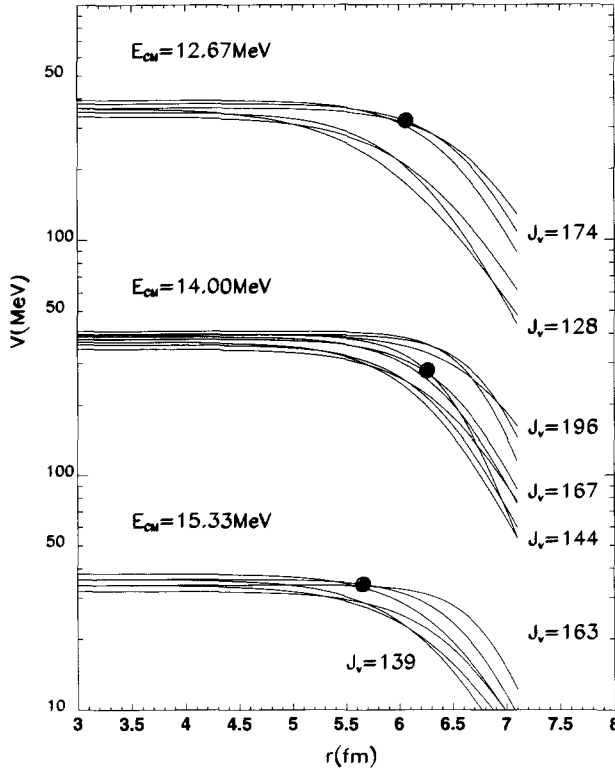
Fig. 5. Some real optical potentials corresponding to the "mountains" discussed in the text and shown in Fig. 4. Potentials that are located on the same "mountain" present crossing points around 5.5–6.0 fm. Each "mountain" is characterized by the real potential's volume integral, which is also indicated on the figure. The only potential family, which fits the data at all three energies is indicated by circles.

was around 5–6 MeV, we can be sure that for all the energy range studied we remain on the same discrete "mountain", on the same discrete potential family, which is the *first* and *unique* in the parameter range we studied and within the constraints we reported (energy independent r_0, r_{i0} and Woods–Saxon form factors). This real potential presents no continuous ambiguity, however the existence of discrete ambiguity for larger V_0 is probable, but was not investigated in this work. Very deep real potentials with a Woods–Saxon radial form factor could also reproduce the observed oscillations (see Fig. 6) if the ratio between their depths also obeyed the condition $W_0/V_0 = 0.01$–0.02.

In recent years the elastic scattering of light systems ($^{12}C+^{12}C$, $^{12}C+^{16}O$, $^{16}O+^{16}O$) at much higher energies (6 MeV/u $\leqslant E \leqslant$ 100 MeV/u) has been successfully analysed using very deep real potentials [19]. The surprising oscillations observed at much lower energy and the attractive feature of finding the first and unique (within the constraints stated above) shallow potential prevented us from exploring the deeper potentials. However, these same data are also being analysed in the framework of deep real potentials in collaboration with Brandan.

The Coulomb potential was calculated treating the projectile as a point and the target

Table 1
Best fit optical potentials of the Potential family II, which is the shallowest and unique within the parameter range studied and constraints considered (see text). The real and imaginary reduced radii are constants and their values are respectively $r_0 = 1.29$ fm and $r_{i0} = 1.77$ fm

| E_{cm} (MeV)	V_0 (MeV)	a (fm)	W_0 (MeV)	a_i (fm)	χ^2
10.67	35.50	0.5	0.138	0.85	10.8
11.33	35.00	0.4865	0.2867	0.825	1.95
12.00	37.69	0.4519	0.4406	0.8	6.98
12.33	37.86	0.4	0.4072	0.8	5.5
12.67	38.47	0.4	0.4862	0.538	9.2
13.00	37.80	0.4	0.5929	0.7359	4.6
13.33	37.64	0.4	0.6209	0.512	9.2
13.67	37.51	0.4	0.6724	0.473	9.4
14.00	37.39	0.4	0.623	0.613	9.2
14.33	37.49	0.4	0.7264	0.746	12.45
14.67	36.60	0.4	0.915	0.492	3.39
15.00	36.70	0.4	0.798	0.391	29.11
15.33	36.42	0.4	0.783	0.443	10.8
15.67	36.00	0.4	0.8021	0.4857	13.3
16.00	35.67	0.4	0.8105	0.4818	18.0
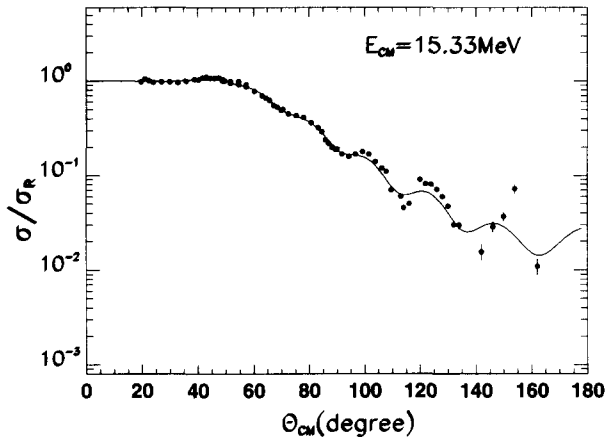
Fig. 6. Experimental elastic scattering angular distribution with optical model fit obtained by the deep potential, whose parameters are $V_0 = 897.2$ MeV , $r_0 = 0.9204$ fm , $a = 0.5178$ fm, $W_0 = 13.52$ MeV, $r_{i0} = 1.128$ fm, $a_i = 0.75$ fm.

as a sphere with the Coulomb radius of $R_C = 1.20A_T^{1/3}$. This Coulomb radius slightly overestimates the Coulomb potential in the interior, when compared to the "sphere + sphere" convention, as was shown by Satchler [20]. However, the conclusions of this work do not depend on the value of R_C we adopted. The Figs. 1–3 present the calculated cross-sections (solid lines) superimposed on the experimental data. The fits are the best for energies between $E_{cm} = 11.33$ and 15.33 MeV, all oscillations being well reproduced, as well in amplitude, as in period and phase. Even at the lowest energy the data were sensitive to the optical potential used in the calculation. At the highest energy ($E_{cm} =$

16.00 MeV), some kind of change occurs. The oscillations in the data are slightly attenuated, when compared to lower energies and the use of the same best fit optical potential family produces oscillations, which are too pronounced. No trivial change, as increasing the imaginary potential depth, or diffuseness could heal this disagreement. It seems as if at $E_{cm} \geqslant 15.67$ MeV the characteristics of the optical potential would undergo some change, some potential family with different characteristics being more appropriate. In a general way however the fits are very satisfactory.

The geometry of the best fit real potential (Pot. II) is fairly standard, $r_0 = 1.29$ fm, thus $R_{opt} = 1.29(A_P^{1/3} + A_T^{1/3}) = 6.674$ fm and $a = 0.40$ fm, while its imaginary part has a very shallow depth with a large radial extension ($r_{i0} = 1.77$ fm) and a large imaginary diffuseness. For some energies a very small imaginary diffuseness also produced comparable fits. The important condition to fit the oscillating angular distributions is the extreme shallowness of the imaginary potential, not only at the surface, but also in the nuclear interior. The ratio W_0/V_0 of this potential is around 0.01–0.02, which is a very low value (ten times smaller than the value for the Maher potential [6]). If this ratio is increased by increasing W_0, the calculation does not predict any oscillations. The total potential $V_C + V_N$ for the lowest energies and for $l = 0$ partial waves presents a barrier of 11.24 MeV (at $R = 8.70$ fm), which is fairly lower than the Coulomb barrier predicted from the Christensen–Winther parametrization and in good agreement with the angular distributions.

The optical potential II also reproduces the main features of the elastic scattering excitation functions at 90°, 140° [21] and at 180° [22], shown in Fig. 7. The 180° excitation function presents pronounced peaks at $E_{cm} = 13.5$, 15.5, and 16.5 MeV. The excitation functions measured recently [21] between $E_{cm} = 10$ and 17 MeV, at 90° and 140° with energy steps of 30 and 50 keV, respectively, are rather smooth with small structures at 13.1, 13.6 MeV, and 16.00 MeV. A statistical cross-correlation analysis of these excitation functions indicates the existence of several correlated structures, which could be attributed to quasi-molecular resonances. The existence of resonances around the Coulomb barrier is a well established fact in lighter-ion systems, as $^{12}C+^{12}C$ and $^{12}C+^{16}O$ [23–26]. More detailed studies of the scattering matrices of the $^{12}C+^{24}Mg$ system, obtained from phase-shift analysis, are under course and probably will give a more definite answer about the existence of resonances.

The physical origin of the oscillations seen in all angular distributions is not clear. One possible interpretation could be the formation of standing waves in the pocket of the total real potential. The shallow imaginary potential does not completely attenuate the wave-function in the nuclear interior (also confirmed by the notch test, see Fig. 8), where reflection can occur on the internal barrier. The interference between the incident and internally reflected wave-functions could produce standing waves in the pocket of the effective potential. An other interpretation could be the existence of shape resonances [23–26].

The unusual feature of these elastic scattering data can also be related to the static quadrupole deformation of the projectile and target. The projectile ^{12}C has an oblate deformation, while the target ^{24}Mg presents a strong prolate deformation. Recent cal-

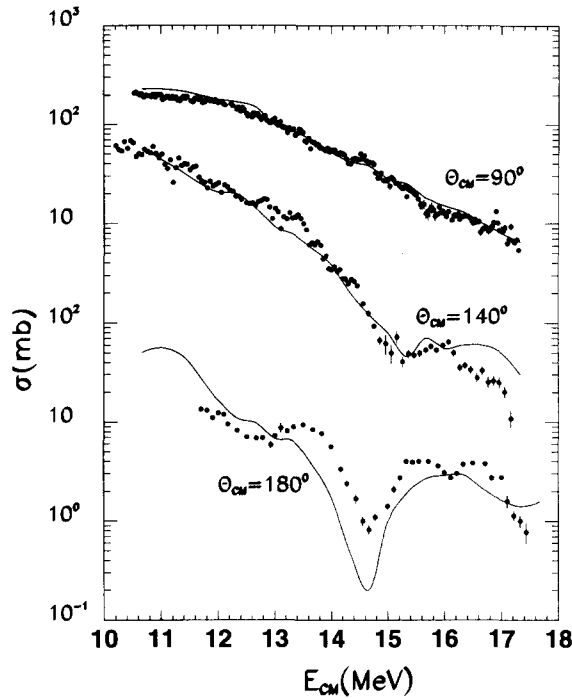Fig. 7. Elastic scattering excitation functions measured at $\theta_{cm} = 90°$, 140° [20] and 180° [21], together with optical model fits using the Potential II of Table 1.

culations of Iwamoto et al. [27] have shown that in the case of the collision between oblate and prolate nuclei, the touching contact can be enhanced, and the fusion barrier be reduced in comparison to the spherical–spherical configuration.

3.1. Notch test analysis

A notch test analysis was performed on several of the angular distributions. A notch, which in this case was a derivative of the Woods–Saxon function (a localised peak), was added to the real part of Pot. II at variable radial positions in order to modify locally the real depth and to observe its effect on the quality of the fit. Whenever the quality of the fit is worsened by the addition of the peak function, there is a sensitivity to the value of the potential depth at this radius. The derivative function had a small diffuseness ($a = 0.3$ fm) and a variable peak height, being always 30% of the real potential depth at the radius considered. The results of the notch test can be observed in Fig. 8.

The addition of the notch produces a worsening of the χ^2 by affecting the amplitude, the period or the phase of the oscillations. This occurs in the radial range between 2 and 8 fm, and consequently proves the sensitivity to the real potential at 2 fm $\leq$ $r \leq 8$ fm. The experimental data are sensitive to the real potential not only in the surface region, as usually happens at higher incident energies, but also in the nuclear
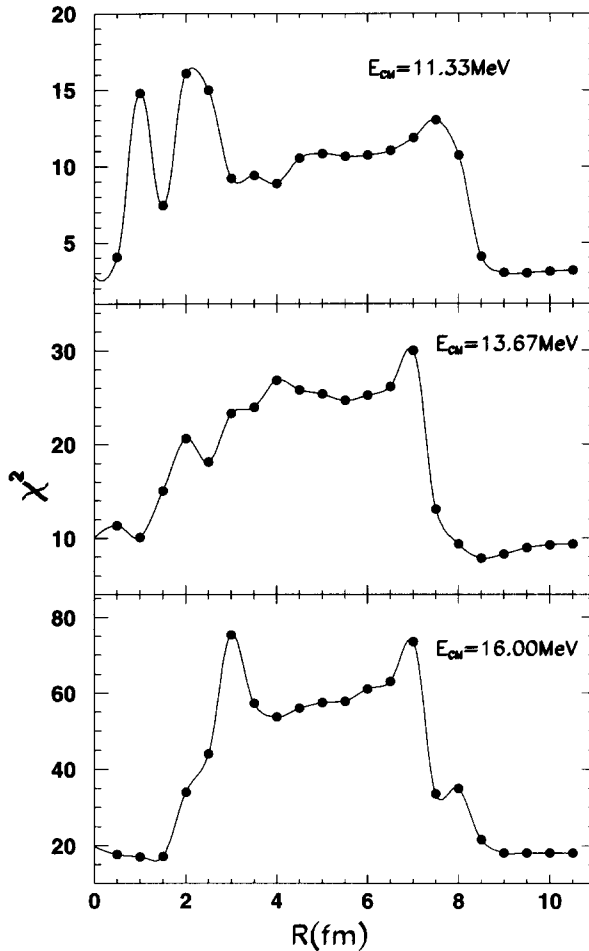
Fig. 8. Notch test of Potential II at some energies.

interior, eliminating any continuous ambiguity in the real potential parameters. It is the very shallow imaginary part of this potential, which allows the penetration of the radial wave-function into the nuclear interior.

The position at 8 fm is 2.3 fm from the sum of the nuclear radii, calculated as $1.1(12^{1/3} + 24^{1/3}) = 5.69$ fm and so corresponds to a region of very low matter density. So it seems that the very low energy elastic scattering probes the nuclear interaction from the nuclear interior out to the very low density region.

3.2. Reaction cross-section

The reaction cross-sections were calculated for the $^{12}C + ^{24}Mg$ system in the energy range between $E_{cm} = 10.67$ and 16.00 MeV, using the best fit optical potentials (Pot. II). In Fig. 9 these results are compared with the available fusion measurements for this
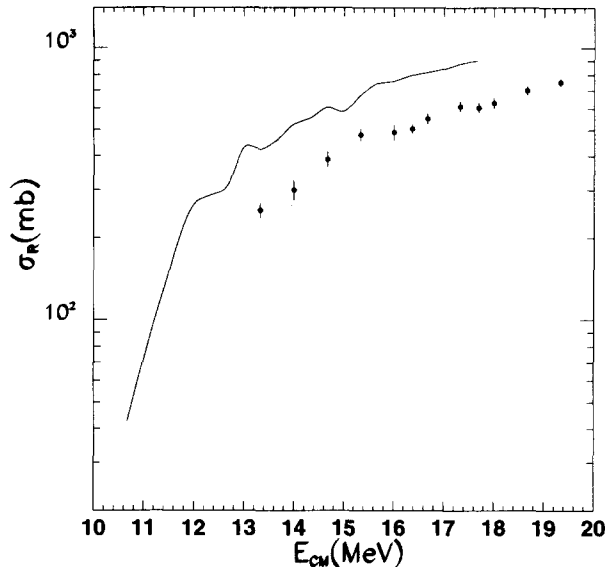
Fig. 9. Experimental fusion cross-sections (dots) for the ^{12}C+^{24}Mg system [27,28], compared with the reaction cross-sections calculated with Potential II (Table 1).

system [28,29]. The experimental fusion cross-sections begin at E_{cm} = 13.2 MeV and if the Coulomb barrier is around 11 MeV as indicated by the present angular distributions no experimental fusion data are available under or near to the Coulomb barrier.

At the available energies the calculated optical model reaction cross-sections are always larger then the experimental fusion. This result is reasonable due to the contribution of the direct reaction processes. Thus, our very shallow imaginary potential predicts reaction cross-sections which exceed the existing fusion data.

4. Threshold anomaly in the elastic scattering

The rapid and localized variation with energy of the real and imaginary depth parameters, also called threshold anomaly behaviour [30], was already verified for many systems [31–33]. It presents two main features: as the incident energy decreases and approaches the Coulomb barrier, the strength of the imaginary potential decreases rapidly. In the same energy range while the energy decreases, the real potential strength first increases, then seems to decrease. However, the experimental evidence for this last decrease is scarce.

The behaviour of $W(E)$ is easily understood in terms of the opening of reaction channels and the subsequent increase in absorption when the Coulomb barrier is overpassed. The energy variation of $V(E)$ is due to the coupling to other channels, represented by the increase in the absorption. These couplings will give rise to corrections to the real potential, which can also be taken into account by dynamical polarization potentials [34]. The threshold anomaly has been well reproduced by calculations using the dispersion

relation between the imaginary and real parts of the optical potential [35,36,30].

For strongly absorbing heavy ion systems, as $^{16}O+^{208}Pb$ or $^{16}O+^{64}Ni$ for example, the sensitivity to the potential is only around a reduced region or point at the nuclear surface, called strong-absorption radius, the crossing radius of the different potentials that fit the data equally well. The dispersion relation calculations are usually performed for the optical potential strength at this radius.

The energy dependence of the real and imaginary depth parameters of our best fit optical potential family (Pot. II) also presents the threshold anomaly, with the imaginary depth decreasing with decreasing energy and the real strength increasing. The strong-absorption radius has no meaning for our unusually transparent optical potential. The notch test has already shown that it is not strongly absorbing in the nuclear interior and the sensitive region is not reduced to a point but is very extended, from 2 to 8 fm. The dispersion relation calculations performed at two points, one around the crossing point ($R = 5.5$ fm) and the other on the surface at 8.5 fm do not reproduce nor quantitatively, neither qualitatively the energy variation of our best fit optical potential at this point.

However, if the dispersion relation is applied to the volume integrals of the real and imaginary parts of the optical potential, the observed energy variation is well reproduced:

$$J_W(E) = \left[\frac{4\pi}{A_T A_P} \int_0^R W(r,E) r^2 \, dr \right] , \tag{2}$$

$$J_{\Delta V}(E) = \frac{P}{\pi} \int_0^\infty \frac{J_W(E')}{E' - E} \, dE' . \tag{3}$$

This can be verified in Fig. 10, where the dots indicate the volume integrals of the best fit optical potentials (Pot. II) as a function of the energy in the center-of-mass frame, and the solid curve is the dispersion relation calculation. This figure also includes higher energy points, at $E_{cm} = 25.26$ and 26.66 MeV, which are taken from Ref. [1].

This feature also corroborates the evidences about sensitivity to the whole nuclear interior or a relative absence of absorption (nuclear transparency) verified at the Coulomb barrier in the case of the $^{12}C+^{24}Mg$ system. The dispersion relation applied to the volume integral has also been used previously in α scattering and in the case of $^{12}C+^{12}C$, at higher energies [37].

4.1. α-transfer polarization potential

At energies twice the Coulomb barrier, the back-angle oscillations in the elastic, inelastic and α-transfer angular distributions and the large structures in the excitation functions observed in many n–α structure systems, as e.g. $^{16}O+^{28}Si$ [10,38], $^{16}O+^{24}Mg$ [10,39,40], could be explained by the explicit inclusion of a dynamical α-transfer polarization potential [38], added to a standard optical potential. At higher energies ($E_{cm} = 25.26$ MeV), the coupling of the α-transfer reaction, $^{24}Mg(^{12}C,^{16}O)^{20}Ne$ has an important role to explain the oscillating elastic scattering data of the $^{12}C+^{24}Mg$
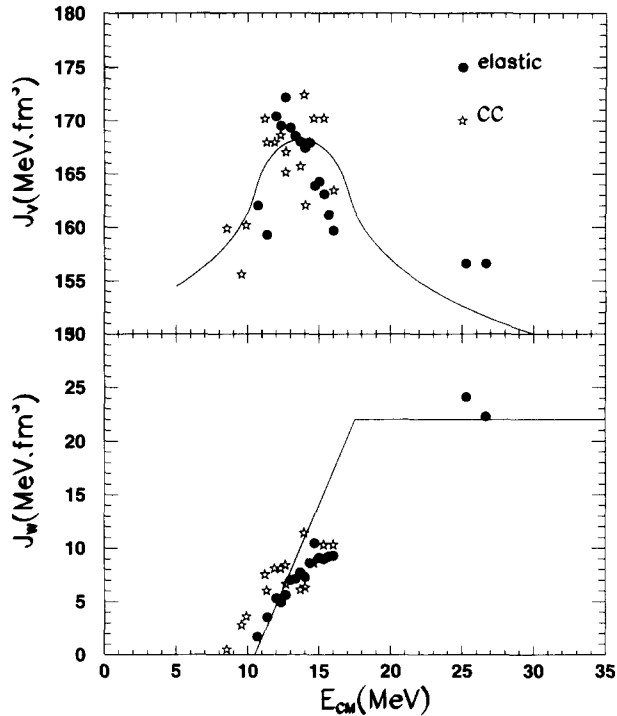
Fig. 10. Volume integrals of the best fit optical potentials (Pot. II) used for the elastic scattering (dots) and for the final excited channels in the Coupled-Channels calculations (stars) as a function of $E_{cm} - Q$. The solid curve is the dispersion relation calculation.

system, as was verified by coupled-channels calculations [41] in the Algebraic Scattering framework [42].

These calculations were also performed at energies around the Coulomb barrier for the $^{12}C+^{24}Mg$ system, adding the polarization potential to a standard strongly absorbing optical potential (E-18). This calculation did not produce oscillating angular distributions at energies near to the Coulomb barrier. Thus, the α-transfer processes cannot explain the oscillations we observed in the $^{12}C+^{24}Mg$ elastic scattering *at the Coulomb barrier*.

The differential cross-section for the $^{24}Mg(^{12}C,^{16}O)^{20}Ne$ α-pickup reaction, was also measured at some energies ($E_{cm} = 12.0$, 13.33, and 16.0 MeV). Its value is around 50 μb/sr at forward angles, that is, somewhat lower, than at higher energies [40]. However, its relative importance when compared to the elastic scattering cross-section, is reduced by at least one order of magnitude due to the increase of the elastic cross-section at low energies.

Landowne and Wolter [13] have also arrived to the conclusion that the effect of two-step α-transfer reaction $^{16}O + ^{24}Mg \rightarrow {}^{20}Ne + {}^{20}Ne \rightarrow {}^{24}Mg + {}^{16}O$ was too small at energies close to the Coulomb barrier.
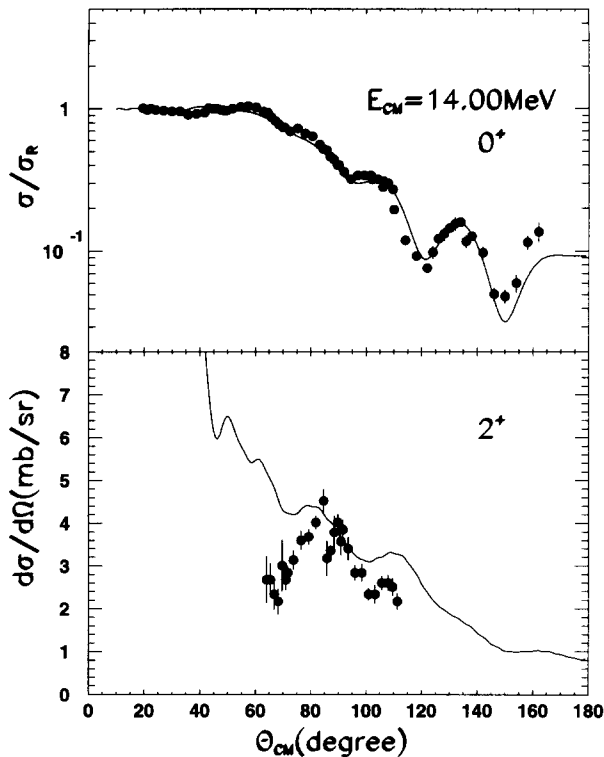
Fig. 11. Elastic and inelastic (2^+) angular distributions fitted with coupled-channels calculations, using the rotational model and $0^+ - 2^+$ coupling for $E_{cm} = 14.00$ MeV.

5. Coupled-channels calculations and threshold anomaly in the inelastic scattering

The ^{24}Mg nucleus is a strongly deformed prolate nucleus and the coupling of the inelastic excitations to the elastic channel can affect the elastic cross-section. We have performed coupled-channels calculations in the context of the rotational model in order to include this coupling. These calculations have been performed using the code ECIS88 [43], assuming a deformed target nucleus and rotational model excitation form factors. In the first step we just coupled the first 2^+ state of ^{24}Mg ($E^* = 1.37$ MeV) to the ground state. The results of these calculations for the data at $E_{cm} = 14.00$ MeV are shown in Fig. 11. In this calculation the same potential II (Table 1) was used for the incoming channel (ground state) and for the exit channel (excited 2^+ state). In order to optimize the fits, we had to reduce the deformation parameters. Instead of the adopted value of the reduced electromagnetic transition probability, $B(E2) = 430$ e^2fm^4 [44], we used 371, and while the more frequently used value of the nuclear deformation length $\delta = \beta R$ is between 1.48 fm [45] and 1.50 fm [11,39], we used in our calculation $\delta = 1.34$ and 1.38 fm, respectively, for the real and imaginary parts. The coupling of the 2^+ state has no strong effect on the elastic scattering angular distributions. The inelastic angular distribution, on the other hand, was very poorly reproduced by this
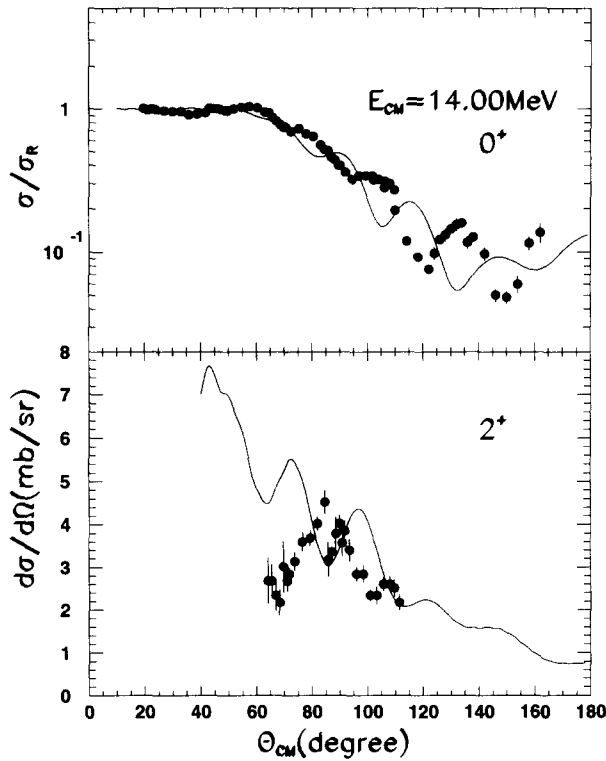
Fig. 12. Coupled-channels calculations with $0^+ - 2^+ - 4^+$ coupling and assuming the same optical potential (Pot. II) in the incoming and outgoing channels (neglect Q-dependence) for $E_{cm} = 14.00$ MeV.

calculation, and could not be improved with reasonable variations of the parameters.

The inclusion of the 4^+ excited state of the ^{24}Mg at $E^* = 4.12$ MeV in the coupled-channels calculation could affect strongly the results for the 2^+ inelastic scattering. For this reason, even if the cross-section of the 4^+ excited state was not computed in our data analysis, we included the 4^+ state in the coupled-channels rotational model calculations in order to improve the agreement between the inelastic data and calculations. The 4^+ state was assumed as a pure rotational band state, with the same quadrupole deformation parameter β_2 for the $0^+ \rightarrow 2^+$ transition and the $2^+ \rightarrow 4^+$ and with no direct excitation from the ground state. The inclusion of the 4^+ state produced a strong shift in the calculated angular oscillations, as well for the elastic and for the inelastic 2^+ scattering (see Fig. 12), when the same optical potentials were used in the incoming (ground-state) and outgoing (2^+ and 4^+ states) channels.

Using the same optical potentials in all channels means not to take the Q-value of the outgoing channels into account in the energy dependence of the optical potentials. In order to consider the kinetic energy disponible in any channel, the Q-value of the channel state has to be subtracted from E_{cm}. In this case, the optical potential to be used in the outgoing channel (with a Q-value) is the one corresponding to the energy $E_{cm} - Q$.

Table 2
Deformation lengths $\delta = \beta R$ and electric transition probability $B(E2)$ used in the coupled-channels calculations

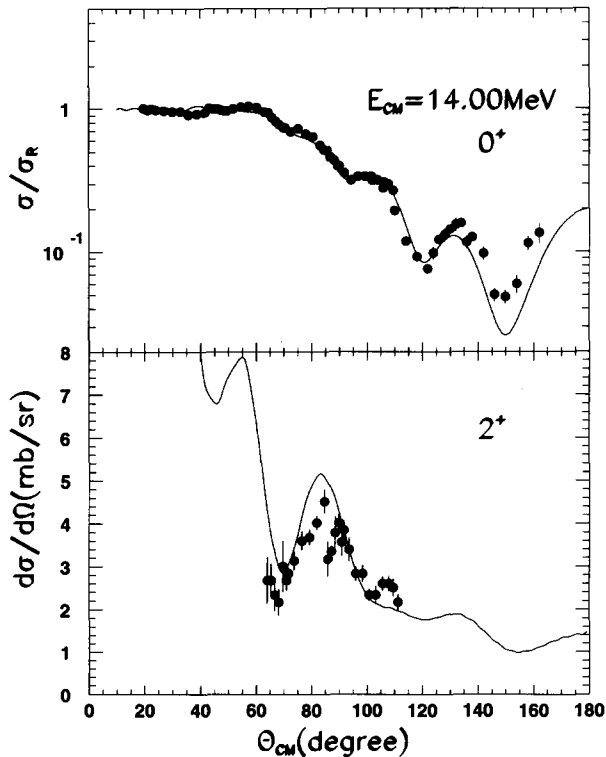| E_{cm} (MeV)	δ_2^{Nr} (fm)	δ_2^{Ni} (fm)	$B(E2 \uparrow)$ (e^{2}fm^4)
13.67	1.11	1.38	371
14.00	1.34	1.38	371
15.33	1.36	1.38	371
16.00	1.36	1.38	371

Fig. 13. Coupled-channels calculations with $0^+ - 2^+ - 4^+$ coupling and taking into account the Q-value of the final states in the energy dependence of the optical potentials for $E_{cm} = 14.00$ MeV.

This effect was particularly strong for the $E_{cm} = 14.00$ MeV angular distribution, because this energy corresponds to the top of the bell shaped peak in the energy dependence of the real potential, and the subtraction of the Q-value from the energy changes the real and imaginary potentials on the threshold anomaly curve of Fig. 10. When the Q-value of the outgoing channels was taken into account in the energy dependence of the optical potential, that is, $Q = 1.37$ MeV was subtracted from the energy for the 2^+ state and $Q = 4.12$ MeV was subtracted from the energy for the 4^+ state, the calculated oscillations were again in good agreement with the experimental data. Using these values as starting point, the inelastic and elastic angular distributions
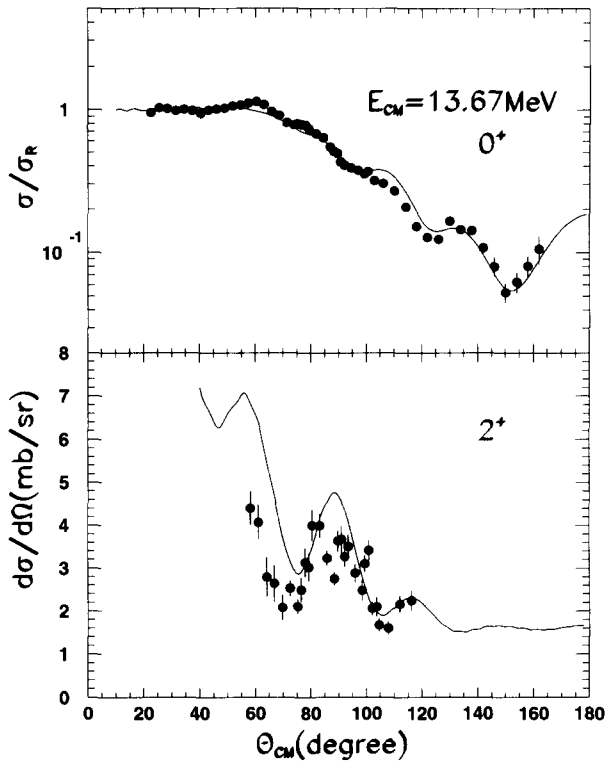
Fig. 14. Coupled-channels calculations with $0^+ - 2^+ - 4^+$ coupling and taking into account the Q-value of the final states in the energy dependence of the optical potentials for $E_{cm} = 13.67$ MeV.

were fitted allowing variations in the optical potentials of the excited channels. In Figs. 13–16 we show the best fits for the $E_{cm} = 14.00$, 13.67, 15.33, and 16.00 MeV elastic and inelastic data. The deformation parameters used are shown on Table 2.

The fits are good, the quality of the elastic fits is not changed by the inclusion of couplings, and the fits of the inelastic excitations are much improved when the 4^+ state is included in the calculations. We can reproduce in detail the various oscillations observed in the experimental data, that constituted a puzzle even before the elastic oscillations [11,12]. The origin of the oscillations seems to be the same as those observed in the elastic scattering, probably being due to the interference of barrier reflected and incident waves.

The best fit potentials used for the excited final states are shown on Table 3, and the volume integrals of these potentials are included in Fig. 10, represented by stars. They follow the same behaviour of the threshold anomaly of the elastic scattering, when the energy is decreased due to the Q-value, J_W is also decreased and J_V increases, for $E_{cm} - Q \geqslant 11.0$ MeV (or decreases, for $E_{cm} - Q \leqslant 11.0$ MeV). We obtain a strong decrease in the real potential intensity for decreasing energies at the Coulomb barrier (11 MeV), which is always foreseen by dispersion relation calculations but usually not observed in experimental data.
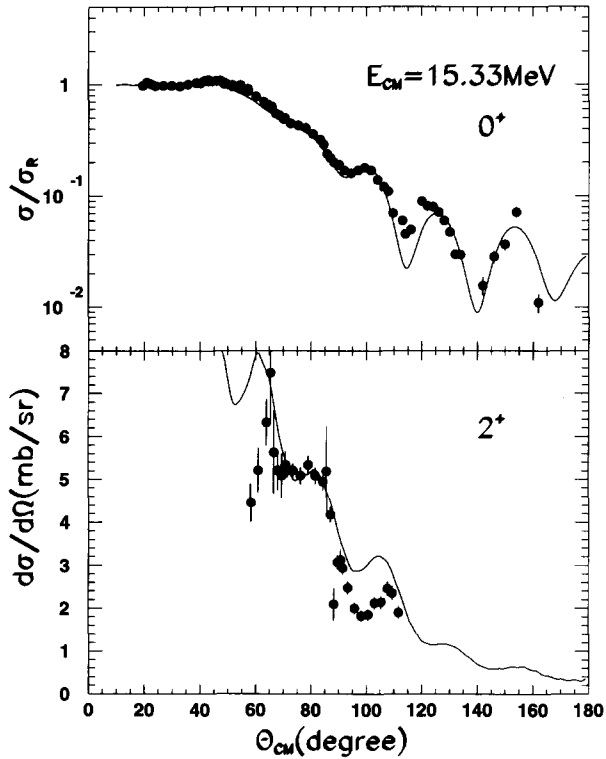
Fig. 15. Coupled-channels calculations with $0^+ - 2^+ - 4^+$ coupling and taking into account the Q-value of the final states in the energy dependence of the optical potentials for $E_{cm} = 15.33$ MeV.

Table 3
Best fit optical potentials of the excited states used in the coupled-channels calculations, indicating the energy E_{cm}, the J^π and Q-value of the states and $E_{cm} - Q$, used to evaluate the energy dependence of the optical model parameters (see text for details)

| E_{cm} (MeV)	J^π	Q (MeV)	$E_{cm} - Q$	V_0 (MeV)	a (fm)	W_0 (MeV)	a_i (fm)
13.67	0^+	0	13.67	37.0	0.4	0.53	0.4726
13.67	2^+	1.37	12.30	37.659	0.4	0.7	0.5
13.67	4^+	4.12	9.55	34.097	0.5	0.23	0.8
14.00	0^+	0	14.00	36.174	0.4	0.5359	0.613
14.00	2^+	1.37	12.63	36.87	0.4	0.7	0.8
14.00	4^+	4.12	9.88	34.3	0.6	0.3	0.8
15.33	0^+	0	15.33	38.0	0.4	0.9	0.4429
15.33	2^+	1.37	13.96	38.5	0.4	1.0	0.4429
15.33	4^+	4.12	11.21	38.0	0.4	0.66	0.4429
16.00	0^+	0	16.00	36.5	0.4	0.9	0.48179
16.00	2^+	1.37	14.63	38.0	0.4	0.75	0.4818
16.00	4^+	4.12	11.88	37.5	0.4	0.7	0.55
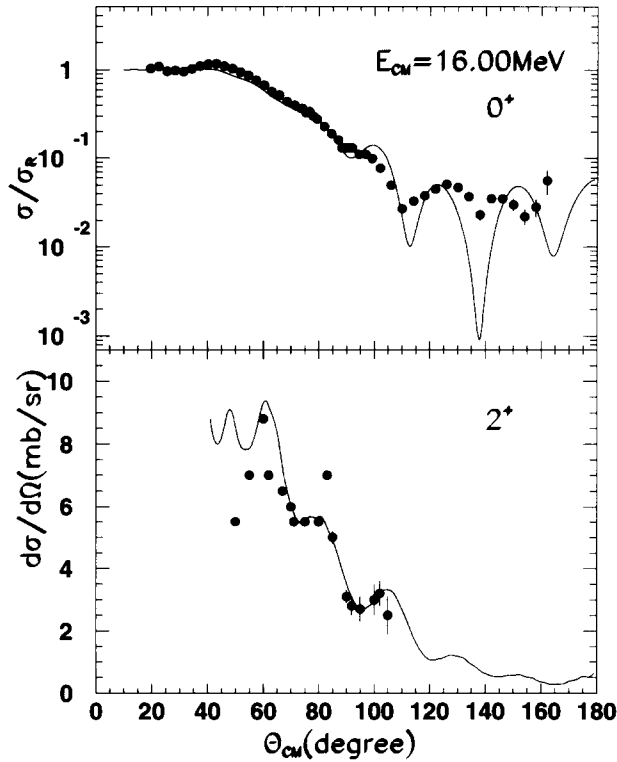
Fig. 16. Coupled-channels calculations with $0^+ - 2^+ - 4^+$ coupling and taking into account the Q-value of the final states in the energy dependence of the optical potentials for $E_{cm} = 16.00$ MeV.

We can conclude that the elastic and inelastic angular distributions are well fitted by these coupled-channels calculations, including the excitation of the 2^+ and 4^+ states of the ^{24}Mg target nucleus and using our best fit optical potential family with the strong threshold anomaly in its energy dependence, as well in the incoming as in the outgoing channels. For the first time a strong Q-value dependence of the optical potential, consistent with the threshold anomaly, was verified for the inelastic scattering. The inclusion of the two first excited states does not eliminate the threshold anomaly of our potential, fact that may indicate that these are not the channels that produce the polarization potential, responsible for the energy variation of the real potential.

6. Conclusions

The complete elastic scattering angular distributions of the ^{12}C+^{24}Mg system were measured at fifteen energies near to the Coulomb barrier between $E_{cm} = 10.67$, and 16.00 MeV. All angular distributions present strong oscillations, and they could not be fitted simultaneously by previously used Woods–Saxon optical potential families with simple energy dependence and normal absorption.

The only shallow ($V_0 \leqslant 45$ MeV) optical potential family that could reproduce the whole amount of data has a very reduced imaginary depth. The condition to reproduce the observed oscillations is that the ratio between the imaginary and real depths cannot exceed 0.01–0.02. Due to this very shallow imaginary potential, the radial wave-functions are not completely attenuated in the nuclear interior. The calculated cross-section, its oscillations, their period and phase are sensitive to details of the real potential at the nuclear surface and in the nuclear interior.

We could determine the real potential ($V_0 \sim 37$ MeV) which is unique, within the constraints of constant geometry and Woods–Saxon form-factor, in the range between 10 MeV $\leqslant V_0 \leqslant 45$ MeV and presents no continuous ambiguity. It is the first and shallowest Woods–Saxon real potential (Pot II), that can fit all angular distributions of the ^{12}C+^{24}Mg system at energies near to the Coulomb barrier.

A notch test performed with potential II showed a sensitivity to the real potential between 2 and 8 fm. The very low energy elastic scattering probes the interaction from the nuclear interior out to regions of very low density. This property could make it a powerful tool to study the interaction potential of exotic halo nuclei, as ^{11}Li, ^{11}Be or ^{14}Be, which present a far extending low-density neutron halo structure.

The volume integrals of this optical potential present the threshold anomaly, which can be well reproduced by dispersion relation calculations. Even the optical potentials used in the excited exit channels of the coupled-channels calculation do present the threshold anomaly, and the Q-value has to be subtracted from their center of mass energy, in order to fit the elastic and inelastic data. We also observed a clear decrease in the real potential depth for decreasing energies at $E_{cm} - Q \sim V_{CB} \sim 11$ MeV, always predicted by calculations but not observed in most cases.

The lowering of the Coulomb barrier, verified in our data, may be related to the deformation of both collision partners: presenting an oblate projectile and a prolate target. Recent work of Iwamoto et al. [27] has shown that deformation and orientation of colliding nuclei have a very significant effect on the height of the barrier and on the compactness of the touching configuration.

Acknowledgements

References

[1] A. Lépine-Szily, W. Sciani, Y.K. Watari, W. Mittig, R. Lichtenthaler, M.M. Obuti, J.M. Oliveira Jr. and A.C.C. Villari, Phys. Lett. B 304 (1993) 45.
[2] R.H. Siemssen, H.T. Fortune, R. Malmin, A. Richter, Y.W. Tippie and P.P. Singh, Phys. Rev. Lett. 25 (1970) 536.
[3] R.H. Siemssen, H.T. Fortune, A. Richter and J.W. Tippie, Phys. Rev. C5 (1972) 1839.

[4] V. Shkolnik, D. Dehnhard and M.A. Franey, Phys. Rev. C 28 (1983) 717;
    V. Shkolnik, D. Dehnhard, S. Kubono, M.A. Franey and S. Tripp, Phys. Lett. B 74 (1978) 195.
[5] C.M. Cheng, J.V. Maher, W. Oelert and F.D. Snyder, Phys. Lett. B 70 (1977) 304.
[6] J.V. Maher, M.W. Sachs, R.H. Siemssen, A. Weidinger and D.A. Bromley, Phys. Rev. 188 (1969) 1665.
[7] W. Reilly, R. Wieland, A. Gobbi, M.W. Sachs and D.A. Bromley, Nouv. Cim. A 13 (1973) 897.
[8] W. Reilly, R. Wieland, A. Gobbi, M.W. Sachs, J. Maher, R.H. Siemssen, D. Mingay and D.A. Bromley, Nouv. Cim. A 13 (1973) 913.
[9] W. von Oertzen and H.G. Bohlen, Phys. Rep. C 19 (1975) 1.
[10] P. Braun-Munzinger and J. Barrette, Phys. Rep. C 87 (1982) 209.
[11] J. Carter, R.G. Clarkson, V. Hnizdo, R.J. Keddy, D.W. Mingay, F. Osterfeld and J.P.F. Sellschop, Nucl. Phys. A 273 (1976) 523.
[12] J. Carter, R.G. Clarkson, V. Hnizdo and J.P.F. Sellschopp, Nucl. Phys. A 297 (1978) 520.
[13] S. Landowne and H.H. Wolter, Nucl. Phys. A 323 (1979) 161.
[14] M.C. Mermaz, E.R. Chavez-Lomeli, J. Barrette, B. Berthier and A. Greiner, Phys. Rev. C 29 (1984) 147.
[15] A.M. Kobos and G.R. Satchler Nucl. Phys. A 427 (1984) 589.
[16] D. Dehnhard, V. Shkolnik and M.A. Franey, Phys. Rev. Lett. 40 (1978) 1549.
[17] P.R. Christensen and A. Winther, Phys.Lett. B 65 (1976) 19.
[18] M.H. Macfarlane ans S.C. Pieper, Argonne National Laboratory Report, ANL76-11 (unpublished).
[19] M.E. Brandan and G.R. Satchler, Physics Report, in press.
[20] G.R. Satchler, Direct Nuclear Reactions (Oxford University Press, 1983) p. 459.
[21] P. Fachini and R. Lichtenthaler, private communication.
[22] M.C. Mermaz, A. Greiner, B.T. Kim, M.J. Levine, E. Muller, M. Ruscev, M. Petrascu, M. Petrovici and V. Simion, Phys. Rev. C 24 (1981) 1512.
[23] D.A. Bromley, J.A. Kuehner and E. Almquist, Phys. Rev. Lett. 4 (1960) 365.
[24] D.E. Groce and G.P. Lawrence, Nucl. Phys. 67 (1965) 277.
[25] J.R. Patterson. B.N. Nagorcka, G.D. Symons and W.M. Ink, Nucl. Phys. A 165 (1971) 545.
[26] R.E. Malmin, R.H. Siemssen, D.A. Sink and P.P. Singh, Phys. Rev. Lett. 28 (1972) 1590.
[27] A. Iwamoto, P. Moeller, J.R. Nix and H. Sagawa, Nucl. Phys. A 506 (1996) 329.
[28] S. Gary and C. Volant, Phys. Rev. C 25 (1982) 1877.
[29] K. Daneshvar, D.G. Kovar, S.J. Krieger and K.T.R. Davies, Phys. Rev. C 25 (1982) 1342.
[30] G.R. Satchler, Phys. Rep. 199 (1991) 147.
[31] J.S. Lilley, B.R. Fulton, M.A. Nagarajan, I.J. Thompson and D.W. Banes, Phys. Lett. B 151 (1985) 181.
[32] B.R. Fulton, D.W. Banes, J.S. Lilley, M.A. Nagarajan and I.J. Thompson, Phys. Lett. B 162 (1985) 55.
[33] D. Pereira, G. Ramirez, O. Sala, L.C. Chamon, C.A. Rocha, J.C. Acquadro and C. Tenreiro, Phys. Lett. B 220 (1989) 347.
[34] W.G. Love, T. Terasawa and G.R. Satchler, Nucl. Phys. A 291 (1977) 183.
[35] C. Mahaux and H. Ngô, Nucl. Phys. A 378 (1982) 205.
[36] M.A. Nagarajan, C. Mahaux and G.R. Satchler, Phys. Rev. Lett. 54 (1985) 1136.
[37] M.E. Brandan, M. Rodriguez-Villafuerte and A. Ayala, Phys. Rev. C 41 (1990) 1520.
[38] M.S. Hussein, A.N. Aleixo, L.F. Canto, P. Carrilho, R. Donangelo and L.S. de Paula, J. Phys. G 13 (1987) 967.
[39] R. Lichtenthaler, A. Lépine-Szily, A.C.C. Villari and O. Portezan, Phys. Rev. C 39 (1989) 884.
[40] A. Lépine-Szily, R. Lichtenthaler, M.M. Obuti, J.M. Oliveira Jr., O. Portezan Filho, W. Sciani and A.C.C. Villari, Phys. Rev. C 40 (1989) 681.
[41] A. Lépine-Szily, M.M. Obuti, R. Lichtenthaler, J.M. Oliveira Jr. and A.C.C. Villari, Phys. Lett. B 243 (1990) 23.
[42] Y. Alhassid, F. Iachello and B. Shao, Phys. Lett. B 201 (1988) 183;
    Y. Alhassid and F. Iachello, Nucl. Phys. A 501 (1989) 585.
[43] J. Raynal, Report IAEA-SMR 9/8 (1988).
[44] A. Christy and O. Hausser, Nucl. Data Tables A 11 (1973) 281.
[45] W.J. Thompson and J.S. Eck, Phys. Lett B 67 (1977) 151.